J Mater Sci (2006) 41:7454–7458
DOI 10.1007/s10853-006-0798-9

In-situ X-ray-diffraction studies of hydrogenated nanocrystalline gadolinium films

E. Shalaan · K.-H. Ehses · H. Schmitt

Received: 19 May 2005 / Accepted: 1 December 2005 / Published online: 20 September 2006

Abstract There is a great deal of interest in ultra-fine grained and nanocrystalline microstructure as a means of achieving enhanced strengths and interesting combinations of properties. Thin Pd-capped rare-earth metallic films switch reversibly from their initial reflecting state (metal phase) to visually transparent state (insulator or semiconductor phase) when exposed to gaseous hydrogen. Reversion to the reflecting state is achieved by exposure to air. Palladium-capped nanocrystalline gadolinium films with different grain sizes were prepared by rf-sputtering technique. Exposure of these metallic films to hydrogen resulted in formation of hydrides and increased disorder. The microstructure of the nc-Gd films were characterized by in-situ X-ray-diffraction studies during hydrogen loading. The grain size, the microstrain, and the lattice parameters were determined.

Introduction

A remarkable discovery by Huilberts et al. [1], initiated interest in metal hydride optical switches smart windows. When the hydrogen content in palladium-capped (5–20 nm) yttrium and lanthanum films (200–500 nm) was varied with H_2 pressure, they switched reversibly from opaque metal at lower hydrogen content to transparent semiconductor at high hydrogen content. Chemically the reaction can be described by Eq. 1:

$$\mathrm{Gd} + 1\mathrm{H_2} \overset{\mathrm{Pd}}{\Longrightarrow} \mathrm{GdH_2} + \frac{1}{2}\mathrm{H_2} \Longleftrightarrow \mathrm{GdH_3} \qquad (1)$$

At room temperature, the first part of the reaction is irreversible, the second part of the reaction from Gd-dihydride to Gd-trihydride is reversible and can be used in a smart window arrangement. The Pd cap prevents oxidation and catalyzes hydrogen absorption at room temperature. Recently, much progress has been made in developing practical optical devices incorporating metal hydrides [2].

Hydrogen molecules dissociate on catalytic metal surfaces, dissolve atomically into the substructure, and interact with the microstructure of the metals. The interaction depends not only on the hydrogen concentration in the bulk but also on the prevalent microstructure; i.e., the mixture of crystal defects, grain boundaries, grain size, grain orientation, and phase composition present within the metal matrix. The density and blend of these features depends on the manufacturing and operating history of the metal.

In this study, in-situ XRD measurements were performed, on nc gadolinium films with different grain sizes during hydrogen loading. Beside the grain sizes, microstructure parameters such as microstrain and lattice parameters were determined and analyzed.

E. Shalaan (✉) · H. Schmitt
Technical physics, Saarland University, Saarbruecken, Germany
e-mail: eshalaan@yahoo.com

K.-H. Ehses
Experimental Physics, Saarland University, Saarbruecken, Germany

Experimental details

Film production

The nanocrystalline gadolinium films are deposited onto glass substrates by rf-sputtering in Ar atmosphere (2×10^{-5} Pa base pressure, 2 Pa working pressure) at room temperature by use of Gd target with a purity of 99.999%. Some Gd films were prepared under different conditions to obtain a different grain sizes. The parameters changed were working gas pressure and sputtering power. The layer thickness is determined by an oscillating quartz microbalance. All the films used in this work have the same thickness of $d = 300$ nm. Before exposing the films to the ambient, they are covered with a thin palladium cap layer of about 15 nm. The palladium layer protects the gadolinium films from oxidation and to promote H_2 dissociation. The Pd film was grown at room temperature to prevent alloy formation with the gadolinium.

Film characterization

Surface morphologies of the prepared nc-Gd films, before hydrogen loading, were checked by means of an ex-situ atomic force microscopy (AFM), using a Digital Instruments Dimension 3100 operating in contact mode with Si-tips (Nanosensors LFM16, force constant 0.18 N/m, tip radius < 10 nm) [3, 4]. The scanned areas are typically 2×2 and 5×5 μm^2 from which the root mean square (rms) roughness and height distributions are determined.

In order to record the XRD spectra of Gd films in equilibrium with hydrogen at various concentration, we used a special gas loading cell. The sample can be exposed to controlled hydrogen gas atmosphere during the measurements via two tubes connected to a vacuum pump and a hydrogen gas cylinder. The gas loading cell is designed for vacuum, but works also reliably up to normal hydrogen pressure. The cell is also equipped with an electrical feed-through with several pins to permit measurements of the resistivity of a sample during hydrogenation. Since Gd is a metal and GdH_3 is a semiconductor, the time evolution of hydrogenation can be pursued in real time by monitoring the change of the resistivity.

Room temperature XRD measurements were carried out using $CuK_{\alpha 1}$ radiation in a X-ray diffractometer in the $(\theta - 2\theta)$ geometry. The spectra of the films were scanned over the range of 20°–90° (2θ), with a step rate of 0.02° (2θ) and a fixed counting time of 10 s for each step, in order to obtain spectra with sufficient signal-to-noise ratio. A standard Si sample was used to correct d-spacing systematic errors and to estimate the instrumental broadening.

Results and discussions

AFM investigation

Figure 1a and b show AFM images taken for nc-Gd film grown at room temperature. The topographical appearance indicates that the grains have similar size and shape. By performing a roughness analysis on the AFM images shown in Fig. 1, the (rms) surface roughness of the nc-Gd surface is estimated to be about 9 nm, and the maximum height is of order of 90 nm.

XRD diffraction analysis

In order to derive information about the Bragg shapes and the magnitude of the additional noise intensity, the Pseudo-Voigt (pV) function was used to fit the data. The pV function is a linear combination of Lorentzian and Gaussian functions represented by [5]:

$$pV^k(x) = I_o^k\left[\eta^k C^k(x) + (1-\eta^k)G^k(x)\right] \tag{2}$$

where $C^k(x) = (1 + x^2)^{-1}$, and $G^k(x) = \exp[-(\ln(2))x]$, with $x = ((2\theta - 2\theta_o^k)/\omega_k)$, $2\omega_k$ is the full-width at half-maximum (FWHM), η^k (the Cauchy (Lorentz) content) weights the relative amounts of Lorentzian and Gaussian components, such that $\eta = 1$ is the pure Lorentzian and $\eta = 0$ is the pure Gaussian, and $2\theta_o^k$ the position of the peak maximum of the kth intensity peak. The parameters η^k and ω^k were adjusted independently and fitted in the peak profiles of the non-subjects.

The pV function can be conveniently written in terms of the integral breadth of Gaussian (G) and Cauchy (or Lorentz, L) components (β_G and β_L, respectively) as:

$$pV(2\theta) = I_o\left[(1-\eta)\exp\left(-\frac{\pi(2\theta - 2\theta_o)^2}{\beta_G^2}\right) + \eta\left(1 + \frac{\pi^2(2\theta - 2\theta_o)^2}{\beta_L^2}\right)^{-1}\right] \tag{3}$$

The two components (G and L) have been assumed to have the same full width at half maximum (FWHM). An useful property of the pV is that the integral breadth, β, can also be written as a weighted average of the G and L components:

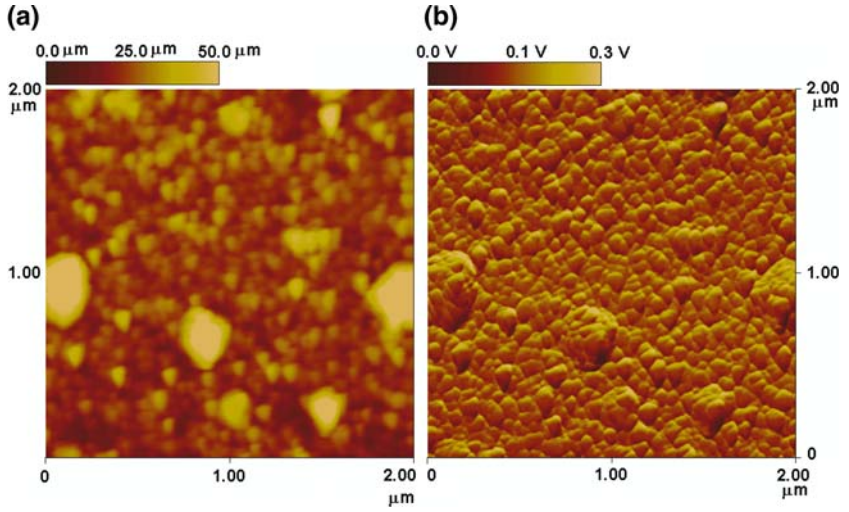

Fig. 1 AFM images showing the microstructure of the surface (2×2 µm^2) of a (300 nm) nc-Gd capped with Pd (15 nm): contact mode (**a**) height and (**b**) friction image

$$\beta = (1-\eta)\beta_G + \eta\beta_L \tag{4}$$

To represent profile asymmetry, the so-called split-*pV* functions, should be used:

$$pV(2\theta) = I_o\left[(1-\eta)\exp\left(-\ln(2)\frac{(2\theta-2\theta_o)^2}{\omega_{l,r}^2}\right) + \eta\left(1+\frac{(2\theta-2\theta_o)^2}{\omega_{l,r}^2}\right)^{-1}\right] \tag{5}$$

where the l and r subscripts refer to the ω (half width at the half maxima, HWHM) for $2\theta < 2\theta_o$ (left-hand side) and $2\theta > 2\theta_o$ (rigt-hand side), respectively.

The shape of the reflections is originated from the broadening profiles of the grain-size refinement, and the microstrain. The microstrain broadening profile is related to the distribution of the microstrain in grains due to dislocations and stacking faults. The analysis of the shape of the peaks for obtaining information about the material is referred to as line profile analysis (LDA). The shapes of line profiles are also affected by instrument and sample shape, which is referred to as instrumental broadening. This instrumental broadening needs to be eliminated to obtain broadening exclusively due to metallurgical effects (e.g., for metallic samples). Once such data is obtained, estimation of coherent domain size, microstrains within these domains, density of dislocation, stacking fault probability etc. can be done.

The correction for instrumental broadening (b) is the most important step in the estimation of material properties from line profile analysis. A careful scan of a suitable standard sample, showing minimal physical broadening will define the instrumental contribution to broadening. The process of abstracting the instrumental function from the sample profile is called *deconvolution*. The reliability of the true profile depends on whether or not the deconvolution is successful. It should be noted that the validity of a deconvolution is in doubt if the peak widths of the standard and investigated samples are comparable.

Integral breadth (b) due to instrumental broadening is defined as ratio of the area under the peak (A) and the maximum intensity (I_o) when the sample is free from the microstructural broadening effects, and it is given by the following equation:

$$b = \frac{\text{FWHM}}{2}\left[(1-\eta)\left(\frac{\pi}{\ln 2}\right)^{1/2} + \eta\pi\right] \tag{6}$$

Because the lines of standard and studied specimen usually do not coincide, it is required to model the characteristic parameters of the standard's line-profile shapes analytically so that the needed instrumental profile can be synthesized at any angle of interest. Most often, the original Caglioti relations is used [6]:

$$(\text{FWHM})^2(2\theta) = u\tan^2\theta + v\tan\theta + w \tag{7}$$

$$\eta(2\theta) = a(2\theta)^2 + b(2\theta) + c \tag{8}$$

where, u, v, w, a, b and c are refinable parameters.

The observed integral breadth (B) in the nc-Gd films (for calculation of D, ρ and ε) is corrected for instrumental broadening (b) to give corrected integral breadth (β) using the following relationship [7]:

$$\beta = B - \left(\frac{b^2}{B}\right) \tag{9}$$

This correction assumes that the peak is somewhat between Gaussian and Cauchy (Lorentzian) that leads to more exact results.

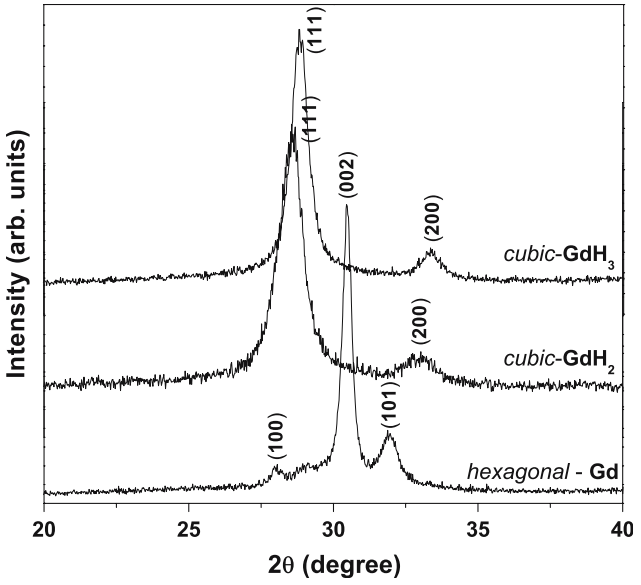

Fig. 2 In-situ XRD spectra of Gd nanocrystalline (300 nm) film before and after hydrogenation (as indicated)

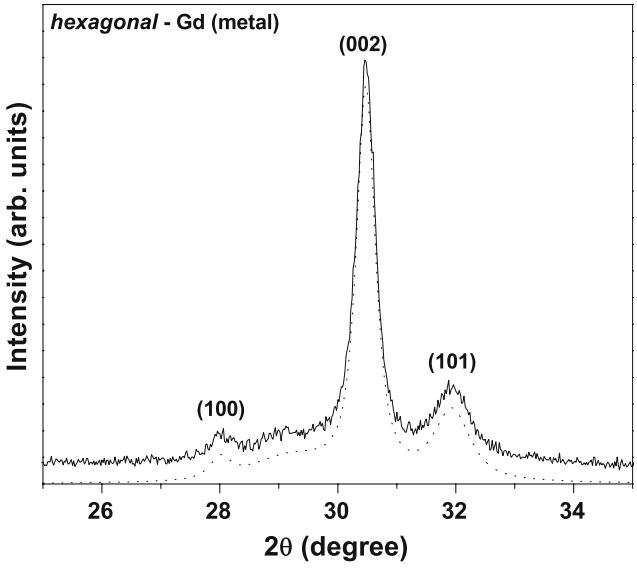

Fig. 3 X-ray diffraction profile of Gd nanocrystalline (300 nm) film: The full line is the observed data. The dotted line is the Bragg reflection profiles fitted by *pV* function after removing the background intensities

According to the analysis above, the mean grain size D, and the mean microstrain ε of the sample can be calculated from the integral width of the physical broadening profile β in terms of Scherrer and Wilson using the following equation [8]:

$$\left(\frac{\beta\cos\theta}{\lambda}\right)^2 = \left(\frac{K}{D}\right)^2 + \left(\frac{4\varepsilon\sin\theta}{\lambda}\right)^2 \quad (10)$$

where β = instrumental corrected broadening (radians), θ = Bragg diffraction angle, λ = wavelength (nm), K is a factor, being taken as 0.9 and D (nm) and ε represent the mean grain size and the mean microstrain, respectively.

The structure of the bulk dihydride gadolinium GdH_2 film are investigated by Ellner et al. [9]. They found that GdH_2 exhibits defect CaF_2 structure with space group $Fm\bar{3}m$. Whereas, the structure of the trihydride GdH_3 is HoH_3 type with space group $P\bar{3}c1$ [10].

Figure 2 shows the XRD spectra of nc-Gd film, before and during hydrogenation.

For metal-Gd film, the spectrum (Fig. 3) suggests a hexagonal structure with a strong preferential orientation along the (002) direction, $2\theta = 30.46°$. The full line is the observed data. The dotted line is the Bragg reflection profiles fitted by pV function after removing the background intensities. By using the peaks data, grain sizes and microstrain can be calculated (Table 1).

The structure of GdH_2 is formed by departing from a hexagonal close-packed substructure of gadolinium and by filling its tetrahedral and a triangular atomic positions with hydrogen atoms. The result is the changing from hexagonal to cubic structure for dihydride phase GdH_2. Figure 4 show the XRD spectrum of GdH_2 film, the reflections at $2\theta = 28.58°$ and 33.027° corresponding to the (111) and (200) planes of the cubic structure, respectively.

As the hydrogen content increases, the film still in cubic phase, with a little shift in Bargg angle (2θ) towards larger values, Fig. 2. For the trihydride phase GdH_3 (Fig. 5) the reflections at $2\theta = 28.82°$ and 33.267° also corresponding to the (111) and (200) planes of the cubic structure, respectively.

Refinement of lattice parameters

The determination of the lattice parameters in Gd films includes two stages. First, the $\lambda_{k\alpha 2}$ component in the X-ray beam should be removed. It enhances the line broadening and introduces asymmetry into the profile. The correct determination of the background counts is critical to successful execution of this procedure and

Table 1 The measured lattice parameters, grain sizes (nm) and microstrains of Gd, film before and after hydrogenation

	Structure	a (Å)	c (Å)	Grain size D (nm)	Microstrain ε (%)
Metal-Gd	Hexagonal	3.678	5.86	80	0.122
GdH_2	Cubic	–	5.415	25	0.122
GdH_3	Cubic	–	5.36	50	0.122

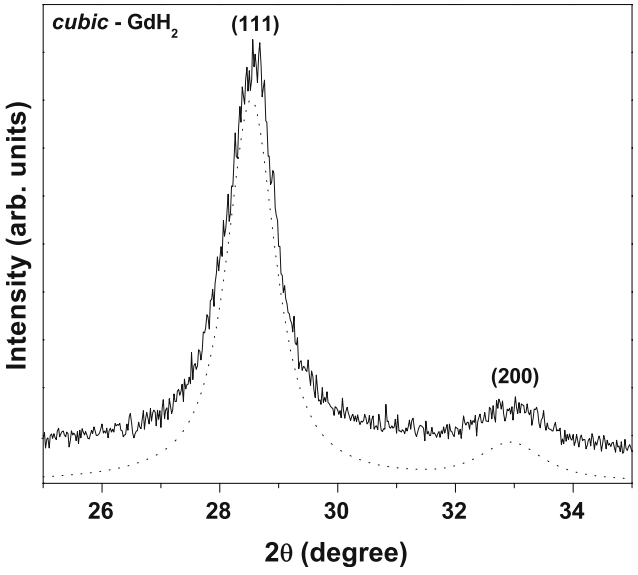

Fig. 4 X-ray diffraction profile of GdH_2 film: The full line is the observed data. The dotted line is the Bragg reflection profiles fitted by *pV* function after removing the background intensities

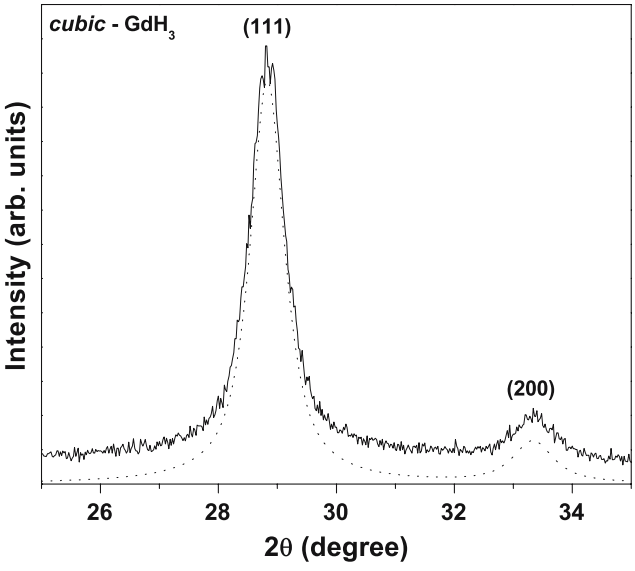

Fig. 5 X-ray diffraction profile of GdH_3: The full line is the observed data. The dotted line is the Bragg reflection profiles fitted by *pV* function after removing the background intensities

subsequent operations, and it should be carefully determined in order to prevent large errors due to peak truncation. The elimination of the $\lambda_{k\alpha 2}$ component is achieved by the use of the modified Rachinger method [11, 12]. Second, the peak positions should be calibrated by external standard method using a pure Si polycrystal in order to minimize the systematic error.

The calculated lattice parameters are shown in Table 1. We note that, the unit cell parameter decreases with increasing hydrogen content from dihydride to trihydride, while the grain size is increases. This is due to the high degree of stacking faults in the nanocrystalline Gd film. The hydrogen atoms fill the defect positions and the interplan spaces.

Conclusion

It has been shown that the hexagonal structure of nanocrystalline metal Gd film changed to cubic phase upon hydrogenation. Transformation from dihydride GdH_2 to trihydride GdH_3 does not change the structure, it is still cubic, only the lattice parameter decreases and the grain size increases. This is due to the high degree of stacking faults in the nanocrystalline Gd films.

Acknowledgements The work is supported by the Deutsche Forschungsgemeinschaft within the GRK: ''Efficient materials for energy conservation,'' which is gratefully acknowledged.

References

1. Huilberts JN, Griessen R, Rector JH, Wijngaarden RJ, Dekker JP, de Groot DG, Koeman NJ (1996) Nature (London) 380:231
2. Armitage R, Rubin M, Richardson T, O'Brien N, Chen Y (1999) Appl Phys Lett 75:1863
3. Yuan H, Lu D-C, Liu X, Chen Z, Han P, Wang X, Wang D (2002) J Cryst Growth 234:77
4. Yuan H, Chen Z, Lu D-C, Liu X, Han P, Wang X (2002) J Cryst Growth 234:115
5. Cox DE, Hastings JB, Cardoso LP, Finger LW (1986) Materials science forum, vol 9. Trans Tech Publications, Aedermannsdorf, Switzerland, p 1
6. Caglioti G, Paoletti A, Ricci FP (1958) Nucl Instrum Methods 3:223
7. Rama P, Anantharaman TR (1963) Z Metallk 54:658
8. Sharp JV, Makin MJ, Christian JW (1965) Phys Status Solidi 11:845
9. Ellner M, Reule H, Mittemeijer EJ (1998) J Alloys Compd 279:179
10. Ellner M, Reule H, Mittemeijer EJ (2000) J Alloys Compd 309:127
11. Labell J, Zagofsky A, Pearlman S (1975) J Appl Crystallogr 8:499
12. Platbrood G (1983) J Appl Crystallogr 16:24